## Topical Application of a PDE4 Inhibitor Ameliorates Atopic Dermatitis through Inhibition of Basophil IL-4 Production



Kazufusa Takahashi<sup>1,2</sup>, Kensuke Miyake<sup>1</sup>, Junya Ito<sup>1</sup>, Hinano Shimamura<sup>1,3</sup>, Tadahiro Suenaga<sup>3</sup>, Hajime Karasuyama<sup>1</sup> and Kenichi Ohashi<sup>2</sup>

Phosphodiesterase 4 inhibitors have been approved for the treatment of atopic dermatitis. However, the cellular and molecular mechanisms underlying their therapeutic effect remain to be fully elucidated. In this study, we addressed this unsolved issue by analyzing the action of difamilast, a novel phosphodiesterase 4 inhibitor, on an oxazolone-induced skin allergic inflammation commonly used as a mouse model of atopic dermatitis. Topical application of difamilast ameliorated skin inflammation in association with reduced IL-4 expression even when the treatment commenced 4 days after the initiation of oxazolone challenge, showing its therapeutic effect on atopic dermatitis. IL-4—deficient mice displayed milder skin inflammation than did wild-type mice, and the difamilast treatment had little or no further therapeutic effect. This was also the case in mice depleted of basophils, predominant producers of IL-4 in the skin lesion, suggesting that difamilast may act on basophils. Notably, basophils accumulating in the skin lesion showed highly upregulated expression of *Pde4b* encoding the B subtype of the phosphodiesterase 4 family. Difamilast suppressed IL-4 production from basophils activated in vitro, at least in part, through inhibition of ERK phosphorylation. Taken together, difamilast appeared to ameliorate atopic dermatitis inflammation through the suppression of basophil IL-4 production in the skin lesion.

Keywords: Allergic inflammation, Difamilast, ERK, Mouse model, PDE4B

Journal of Investigative Dermatology (2024) 144, 1048-1057; doi:10.1016/j.jid.2023.09.272

#### **INTRODUCTION**

Atopic dermatitis (AD) is an inflammatory skin disorder characterized by chronic and recurrent itch and eczema, which affects 15-30% of children and 2-10% of adults in developed countries (Weidinger and Novak, 2016). Although the precise pathogenesis of AD remains to be fully elucidated (Weidinger et al, 2018), type 2 cytokines including IL-4 and IL-13 have been considered to contribute to the development of a certain type of AD as the anti-IL-4Rα antibody dupilumab successfully improved the signs and symptoms of moderate-to-severe AD (Simpson et al, 2016). Currently, the first-line approach for the treatment of AD is the topical antiinflammatory therapy with corticosteroids and calcineurin inhibitors (Thyssen et al, 2020). Recently, topical therapies targeting phosphodiesterase (PDE) 4 and JAK have been shown to be effective in patients with AD (Nakagawa et al, 2020; Saeki et al, 2022a, 2022b), and therefore they are beginning to be used as alternative approach in clinical practice (Guttman-Yassky et al, 2019; Kleinman et al, 2022).

cAMPs function as a key second messenger molecule regulating signal transduction cascades (Maurice et al, 2014). PDE4 catalyzes cAMP degradation and is subdivided into four subfamilies, namely PDE4A, B, C, and D. Inhibition of PDE4 elevates intracellular levels of cAMP, leading to the reduced production of proinflammatory molecules in various cells, including T cells, macrophages, dendritic cells, keratinocytes, and endothelial cells (Li et al, 2018; Schick and Schlegel, 2022). Recent studies have demonstrated that PDE4 inhibitors are effective in the treatments of a wide variety of disorders, such as chronic obstructive pulmonary diseases, psoriasis, and AD (Fabbri et al, 2009; Paller et al, 2016; Papp et al, 2015; Schick and Schlegel, 2022; Tavares et al, 2020). However, the systemic administration of PDE4 inhibitors often causes nausea and emesis as major adverse events (Calverley et al, 2007). Studies using knockout mice have revealed that mice deficient in PDE4D isoform are protective against anesthesia-induced neurological event (Robichaud et al, 2002), whereas mice deficient in PDE4B isoform display alleviated lung allergic inflammation (Jin et al, 2010). Therefore, PDE4B-selective inhibition would be a good strategy for treating inflammatory disorders.

Two PDE4 inhibitors, crisaborole and difamilast, have been approved for the topical treatment of AD in the United States and Japan, respectively (Paller et al, 2016; Saeki et al, 2022a, 2022b). Nevertheless, the cellular and molecular mechanisms underlying their therapeutic effect remain to be

Correspondence: Kensuke Miyake, 1-5-45 Yushima, Bunkyo-ku, Tokyo 113-8510, Japan. E-mail: miyake.mbch@tmd.ac.jp

Abbreviations: AD, atopic dermatitis; BMBA, bone marrow—derived basophil; OX, oxazolone; PDE, phosphodiesterase; RNA-seq, RNA sequencing Received 21 June 2023; revised 21 September 2023; accepted 26 September 2023; accepted manuscript published online 11 October 2023; corrected proof published online 18 November 2023

<sup>&</sup>lt;sup>1</sup>Inflammation, Infection and Immunity Laboratory, Advanced Research Institute, Tokyo Medical and Dental University (TMDU), Tokyo, Japan; <sup>2</sup>Department of Human Pathology, Tokyo Medical and Dental University (TMDU), Tokyo, Japan; and <sup>3</sup>Department of Immunology, Kitasato University School of Medicine, Sagamihara, Japan

fully elucidated. Difamilast inhibits the activity of PDE4, particularly PDE4B subtype (Hiyama et al, 2023), and has been reported to improve signs and symptoms of AD in adult and pediatric patients in the phase 3 clinical trials (Saeki et al, 2022a, 2022b). In the preclinical study, the topical application of difamilast ointment ameliorated the ear thickening and cellular infiltration in a hapten 2,4,6-trinitro-1-chlorobenzene—induced mouse model of AD (Hiyama et al, 2023). Nevertheless, the main cells targeted by difamilast remain ill-defined. In this study, we addressed this issue by investigating the action of difamilast on an oxazolone (OX)-induced skin allergic inflammation commonly used as a mouse model of AD.

#### **RESULTS**

## Difamilast shows a therapeutic effect on skin inflammation in an OX-induced mouse model of AD

Topical application of 1% difamiliast ointment, starting before the first OX challenge, ameliorated the ear swelling, lichenification, excoriation, and neutrophil infiltration in the skin lesion, when compared with the treatment with ointment base alone (Figure 1a-d). Notably, even when the difamilast treatment commenced 4 days after the initiation of OX challenge (Figure 1e), the skin allergic inflammation was ameliorated, judging from the reduction in skin thickening (Figure 1f), lichenification, dermal hyperplasia (Figure 1g), and infiltration of inflammatory cells, particularly neutrophils (Figure 1h). In accordance with the reduced neutrophil accumulation, the production of CXCL1, a neutrophilattracting chemokine, was also significantly diminished in the skin lesion treated with difamilast (Supplementary Figure S1). Thus, the difamilast treatment showed a therapeutic effect on AD-like skin inflammation.

## Difamilast shows little or no further therapeutic effect on the attenuated skin inflammation in IL-4—deficient mice

We found that the level of IL-4 production in the skin lesion was reduced by the difamilast treatment (Figure 2a). On the other hand, IL-13 production was ∼1,000 times lower than that of IL-4, and the difamilast treatment showed no significant effect on the level of IL-13 protein (Figure 2a). As we reported previously (Yamanishi et al, 2020), IL-4-deficient (II4<sup>-/-</sup>) mice showed much milder skin inflammation than wild-type mice in the OX-induced AD model, manifested by the reduction in ear thickening, lichenification, dermal hyperplasia, and neutrophil infiltration, compared with wildtype mice (Figure 2b-d). Notably, the difamilast treatment showed little or no further therapeutic effects in  $II4^{-/-}$  mice unlike in wild-type mice, judging from no significant change in ear swelling, histopathology, and neutrophil infiltration (Figure 2b-d). These observations suggested the possibility that difamilast may ameliorate the skin inflammation through the suppression of IL-4 production in the skin lesion.

# Difamilast shows little or no further therapeutic effect on the attenuated skin inflammation in basophil-depleted mice and basophil-specific IL-4—deficient mice

We previously reported that basophils are the predominant producers of IL-4 in the skin lesion of the OX-induced AD, and the depletion of basophils ameliorated the skin inflammation (Yamanishi et al, 2020). When difamilast ointment was topically applied in OX-challenged mice in which basophils had been depleted by using anti-CD200R3 antibody (clone: Ba160) (Figure 3a–d) or *Mcpt8*<sup>DTR/+</sup> mice treated with diphtheria toxin to deplete basophils (Supplementary Figure S2a–d), little or no therapeutic effect was observed as in the case of *II4*<sup>-/-</sup> mice (Figure 2b–d). This implied that difamilast may act on basophils, leading to the amelioration of skin inflammation.

Given that the number of basophils accumulated in the skin lesion remained unchanged by difamilast-treatment (Figure 1d), we assumed that difamilast may ameliorate the skin inflammation through the suppression of the IL-4 production from skin-infiltrating basophils rather than the inhibition of basophil infiltration. Indeed, basophils isolated from the skin lesion of difamilast-treated mice showed reduced expression of *Il4* compared with basophils from control mice (Figure 3e). In accordance with this, the difamilast treatment showed little or no further therapeutic effect on the attenuated skin inflammation in basophil-specific IL-4—deficient (*Mcpt8*<sup>iCre</sup> *Il4*<sup>fl</sup>) mice (Figure 3f—h). Taken together, difamilast appeared to ameliorate skin inflammation through inhibition of IL-4 production from basophils.

## Difamilast suppresses the production of IL-4 from activated basophils in vitro

Difamilast has been shown to inhibit the enzyme activity of PDE4, preferentially PDE4B (Hiyama et al., 2023). Therefore, we assessed the expression profile of the PDE4 family in basophils. The PDE4 family includes four subtypes (PDE4A, PDE4B, PDE4C, and PDE4D) in both mice and humans (Li et al, 2018; Maurice et al, 2014; Schick and Schlegel, 2022). Bulk RNA sequencing (RNA-seq) analysis revealed that the expression of Pde4b was the highest among the PDE4s in mature basophils isolated from the bone marrow (GEO accession number: GSE206591 [Miyake et al, 2023]) and also in cultured bone marrow-derived basophils (BMBAs) (Figure 4a and b). Importantly, the *Pde4b* expression was upregulated up to 25-fold by the stimulation with cytokines (IL-3 + IL-33) or 6-fold by antigen/IgE stimulation, whereas the expression of other three subtypes remained unchanged or even downregulated (Figure 4c and Supplementary Figure S3a). Reanalysis of the publicly available single-cell RNA-seq datasets (GEO accession number: GSE149121 [Liu et al, 2020]) (Supplementary Figure S4a) revealed that basophils in the skin lesion of the OX-induced AD model predominantly expressed *Pde4b* among the PDE4 family (Figure 4d). Notably, the Pde4b expression was upregulated in basophils isolated from the OX-treated skin, as compared with those isolated from control (ethanol)-treated skin (Figure 4d), suggesting that PDE4B may play a key role in the activation of basophils in the skin lesion.

Indeed, difamilast suppressed the IL-4 production from BMBAs stimulated with cytokines (IL-3 + IL-33) or antigen/ IgE in a dose-dependent manner (Figure 4e and Supplementary Figure S3b). In contrast, the treatment with GEBR-7b, a PDE4D selective inhibitor, had little or no effects on IL-4 production from activated BMBAs (Figure 4e and Supplementary Figure S3b). Moreover, the difamilast

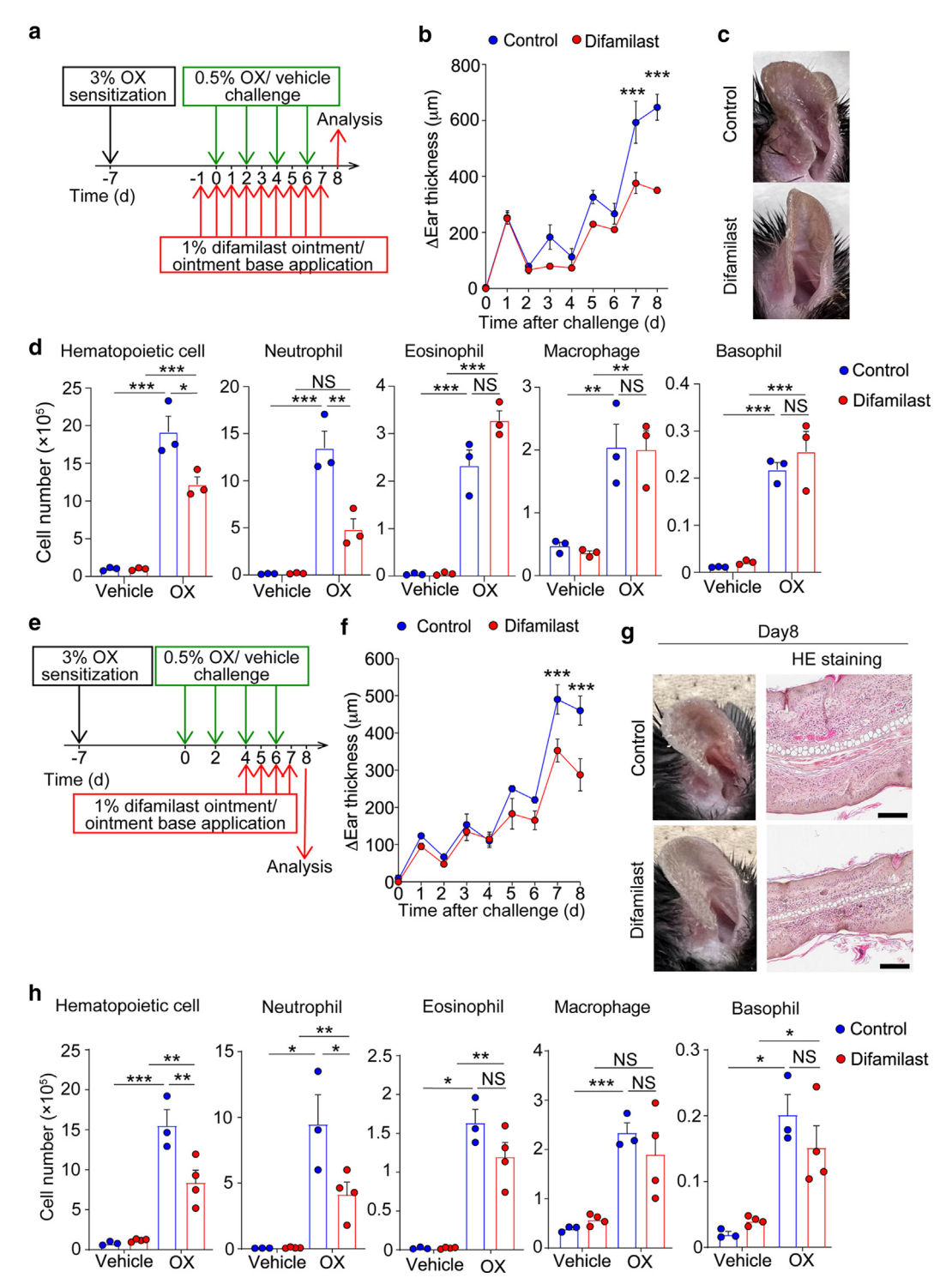


Figure 1. Difamilast exhibits a therapeutic effect on OX-induced AD-like skin inflammation. C57BL/6J mice sensitized with 3% oxazolone (OX) were challenged every other day with topical treatment of 0.5% OX and vehicle alone on their right and left ear, respectively. ( $\mathbf{a} - \mathbf{d}$ ) One percent difamilast ointment or ointment base (as control) was applied daily to both right and left ears starting from 1 day before the first OX challenge. In  $\mathbf{a}$ , the experimental protocol is depicted. In  $\mathbf{b}$ , the time course of ear thickening is shown ( $\Delta$ Ear thickness = OX-vehicle; mean ± SEM, n = 3-4 mice each). In  $\mathbf{c}$ , the gross appearance of the affected ear skin on day 8 is shown. In  $\mathbf{d}$ , the numbers of indicated cell types in the ear skin on day 8 are shown (mean ± SEM, n = 3 mice each). ( $\mathbf{e} - \mathbf{h}$ ) Difamilast or control ointment was applied daily to their ear skin starting after the third OX challenge. In  $\mathbf{e}$ , the experimental protocol is depicted. In  $\mathbf{f}$ , the time course of  $\Delta$ Ear thickness is shown (mean ± SEM, n = 3-4 mice each). In  $\mathbf{g}$ , the gross appearance of the affected ear skin (left panels) and H&E-stained specimens (right panels; Bars indicate 200 μm) on day 8 are shown. In  $\mathbf{h}$ , the numbers of indicated cell types in the ear skins on day 8 are shown (mean ± SEM, n = 3-4 mice each). Data shown in  $\mathbf{b} - \mathbf{d}$  and  $\mathbf{f} - \mathbf{h}$  are representative of at least three independent experiments. \*P < .05, \*\*P < .01, \*\*\*P < .001 measured by two-way ANOVA with Sidak multiple comparison test (for  $\mathbf{d}$  and  $\mathbf{f}$ ) or with Tukey multiple comparison test (for  $\mathbf{d}$  and  $\mathbf{h}$ ). NS, not significant; OX, oxazolone.

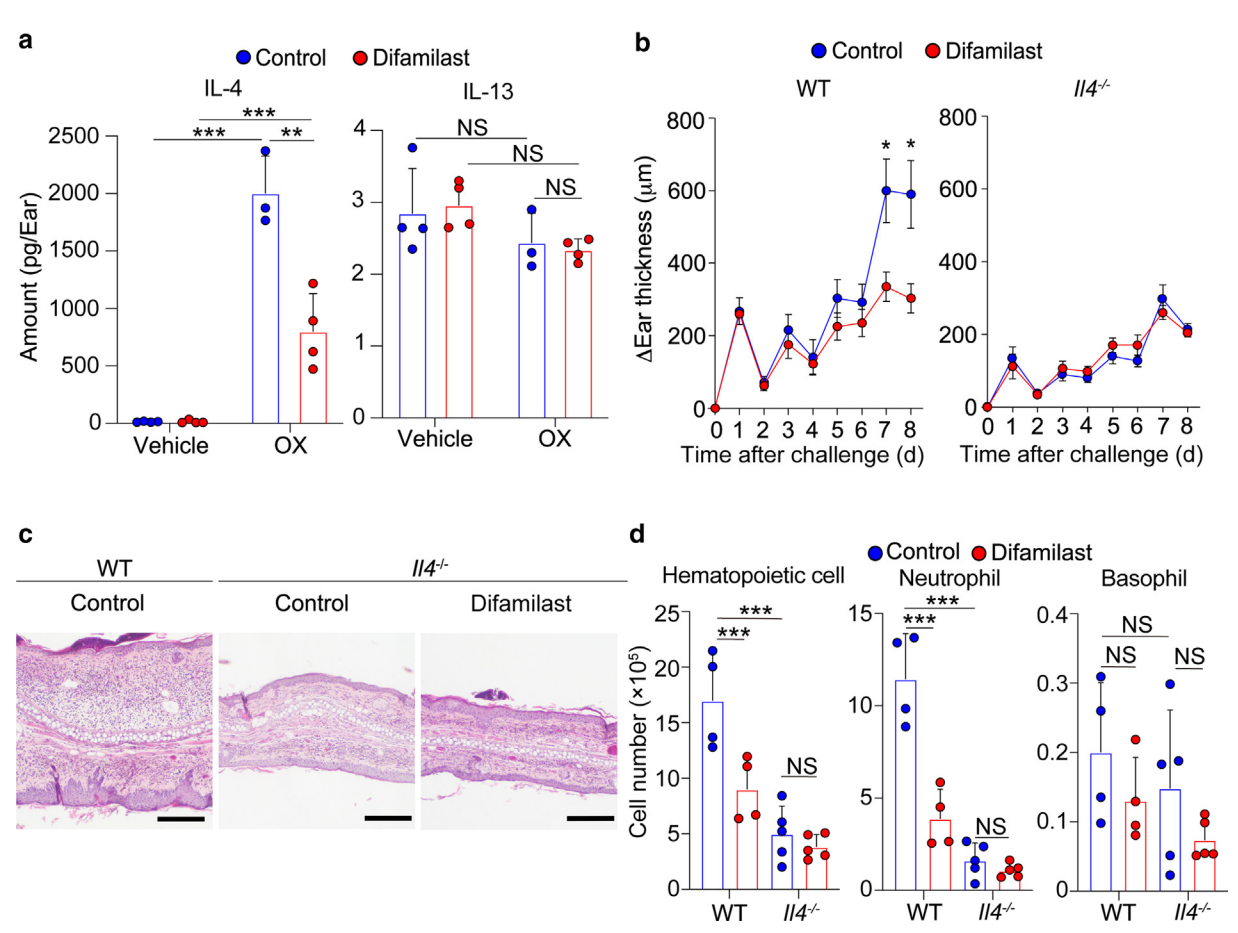


Figure 2. Difamilast shows little or no therapeutic effect on the attenuated skin inflammation in IL-4-deficient mice. C57BL/6J mice were treated as in Figure 1 to induce AD-like skin inflammation. Difamilast or control ointment was applied daily to their ear skin starting after the third OX challenge. (a) The amounts of IL-4 and IL-13 in tissue homogenates collected from the OX-induced skin lesions on day 8 are shown (mean ± SEM, n = 3-4 mice each). (b-d) WT and  $II4^{-/-}$  mice were treated with OX as in Figure 1. Difamilast or control ointment was applied daily to their ear skin starting after the third OX challenge. In b, the time course of ΔEar thickness is shown (mean ± SEM, n = 4-5 mice each). In c, H&E-stained specimens (Bars indicate 200 μm) on day 8 are shown. In d, the numbers of indicated cell types in the ear skin on day 8 are shown (mean ± SEM, n = 4-5 mice each). Data shown in b-d are representative of at least three independent experiments. \*P < .05, \*\*P < .01, \*\*\*P < .001 measured by two-way ANOVA with Tukey multiple comparison test (for a and d) or with Sidak multiple comparison test (for b). NS, not significant; OX, oxazolone; WT, wild-type.

treatment suppressed the activation-induced upregulation of CD63 surface expression which reflects the degranulation (Supplementary Figure S3c and d). Importantly, the difamilast treatment had little effects on the surface expression of the receptors, namely IL-3R $\alpha$ , IL-33R, and Fc $\alpha$ RI on basophils (Supplementary Figure S5a and b), or the viability of basophils (Supplementary Figure S5c). These results clearly demonstrated that difamilast directly acts on basophils to suppress their activation, including the IL-4 production.

## Difamilast interferes with the ERK phosphorylation in activated basophils, leading to the suppression of IL-4 production

To explore the possible mechanisms by which difamilast inhibits the IL-4 production from activated basophils, we conducted bulk RNA-seq analysis of BMBAs treated with difamilast. Transcriptomic analysis revealed that difamilast significantly reduced the gene expression of *II4* and basophil activation marker (*Cd69*) in IL-3 + IL-33—stimulated BMBAs (Figure 5a and Supplementary Figure S6a). Enrichment

analysis uncovered that the genes associated with "ERK1 and ERK2 cascade" and "regulation of ERK1 and ERK2 cascade" were significantly enriched among the genes downregulated by the difamilast treatment (Figure 5b). In contrast, the genes associated with "regulation of inflammatory response" and "regulation of protein serine/threonine kinase activity" were significantly enriched among the genes upregulated by the difamilast treatment (Supplementary Figure S6b). In line with this, the expression of dual specificity phosphatases (Dusp1, Dusp5, and Dusp16), which are known to inhibit ERK phosphorylation (Chen et al, 2019), was significantly upregulated by the difamilast treatment (Supplementary Figure S6c). The treatment with ERK1/2-specific inhibitor (SCH772984) suppressed the IL-4 production from IL-3 + IL-33-stimulated BMBAs (Figure 5c). Given that the difamilast treatment significantly reduced the extent of ERK1/2 phosphorylation in IL-3 + IL-33-stimulated BMBAs (Figure 5d and e), difamilast appeared to suppress the basophil IL-4 production, at least in part, through inhibition of ERK phosphorylation.

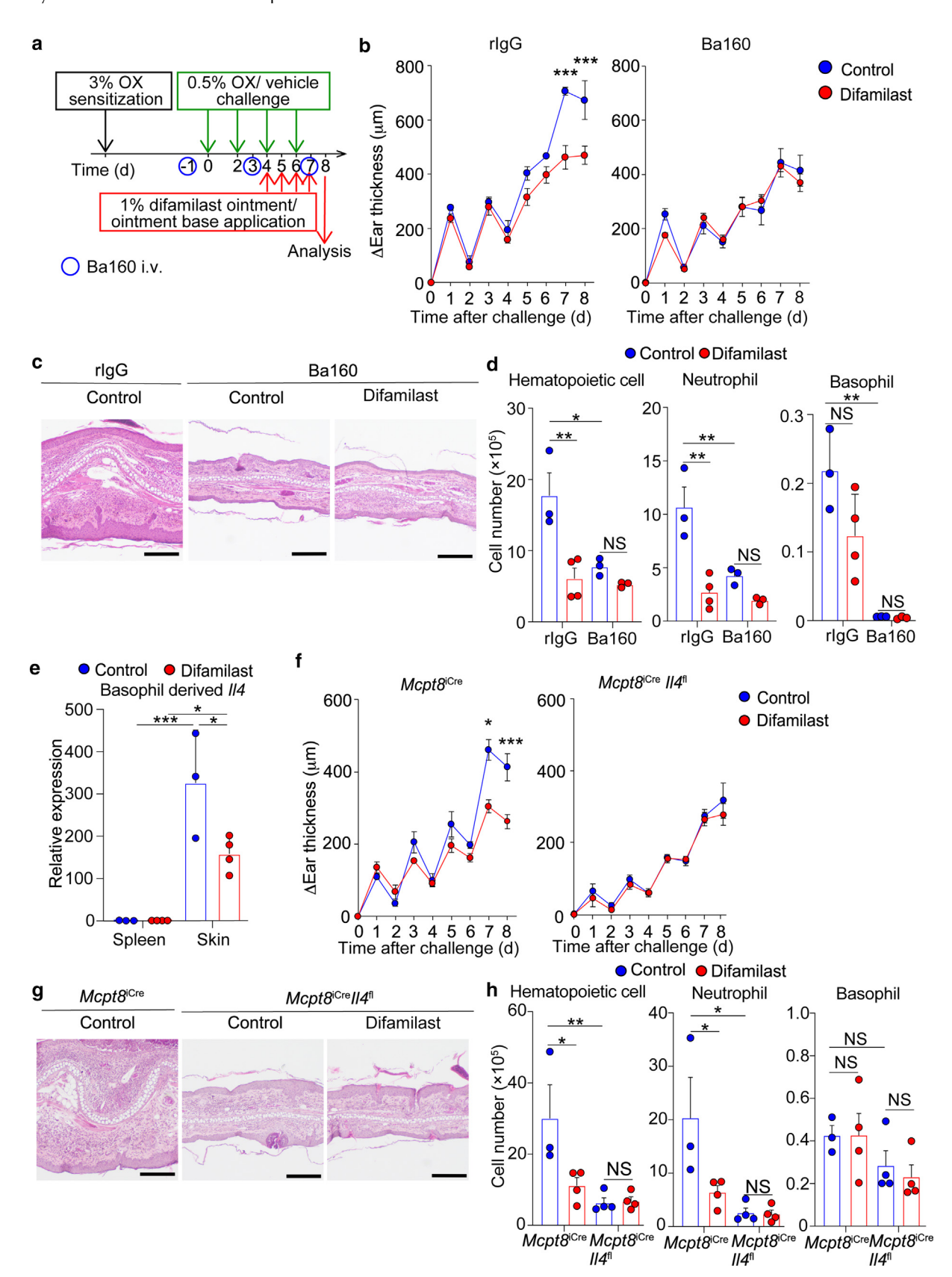


Figure 3. Difamilast has little or no therapeutic effect on the attenuated skin inflammation in basophil-depleted mice and basophil-specific IL-4—deficient mice. (a—d) C57BL/6J mice were treated with OX as in Figure 1. Difamilast or control ointment was applied daily to both right and left ears, starting after the third OX challenge. Basophil-depletion antibody (Ba160; anti-CD200R3 monoclonal antibody), or its isotype-matched control antibody was intravenously administered to mice three times, namely 1 day before, 4 and 7 days after the first OX challenge (as indicated by blue circles). In  $\bf a$ , the experimental protocol is depicted. In  $\bf b$ , the time course of  $\bf \Delta$ Ear thickness is shown (mean  $\bf \pm$  SEM, n = 3 mice each). In  $\bf c$ , the H&E-stained specimens (Bars indicate 200  $\bf \mu$ m) on day 8 are shown. In  $\bf d$ , the number of indicated cell types in the ear skin on day 8 are shown (mean  $\bf \pm$  SEM, n = 3 mice each). (e) WT mice were treated as in Figure 1. The

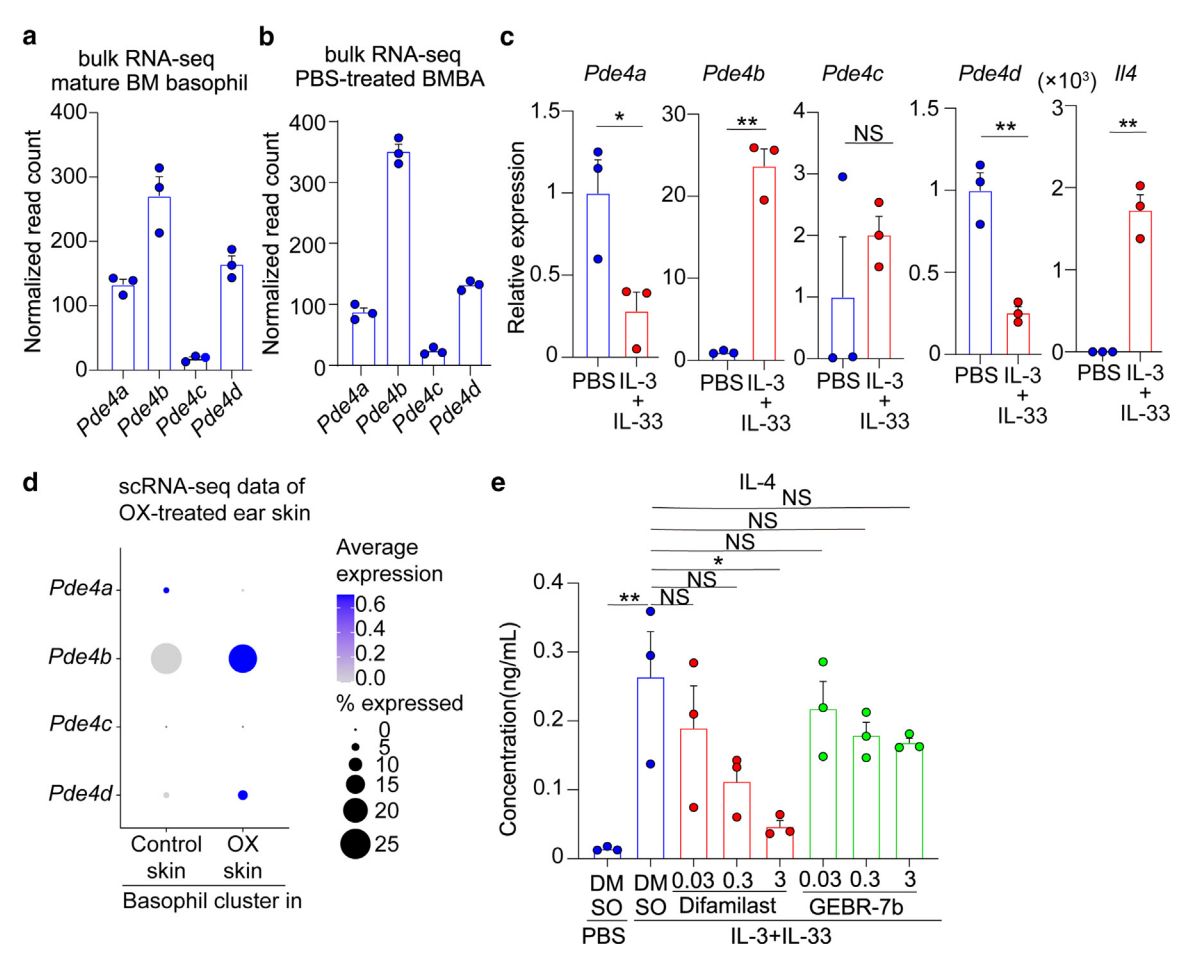


Figure 4. Difamilast inhibits IL-4 production from activated basophils. (a) Bulk RNA-seq data obtained from GSE206591 were reanalyzed. The normalized read counts of four Pde4 subtypes in purified mature basophils from the bone marrow are shown (mean  $\pm$  SEM, n = 3). (b and c) BMBAs were generated by culturing bone marrow cells in the presence of IL-3 for 7 days. They were cultured with IL-3 + IL-33 or control PBS for 4 hours. In b, BMBAs cultured with control PBS were subjected to bulk RNA-seq analysis. The normalized gene counts of four PDE4 subtypes are shown (mean  $\pm$  SEM, n = 3). In c, the mRNA expression of indicated genes in BMBAs stimulated for 4 hours with IL-3 + IL-33 or control PBS is shown. The value of mRNA expression in PBS-treated BMBAs was set as 1. (d) Single-cell RNA-seq data obtained from ethanol-treated or OX-treated skin lesions were re-analyzed (GEO accession number: GSE149121). The mRNA expression of four PDE4 subtypes in basophils detected in ethanol-treated and OX-treated skins is shown in dot plot. The size of the dots indicates the frequency of cells expressing the genes while the color of the dots indicates the average gene expression level. (e) BMBAs were stimulated for 6 hours with IL-3 + IL-33 or control PBS in the presence of varying concentration of difamilast, GEBR-7b or vehicle DMSO alone. IL-4 concentration in BMBA supernatants is shown (mean  $\pm$  SEM, n = 3). Data shown in c and e are representative of at least three independent experiments. \*P < .05, \*\*P < .01, \*\*\*P < .001 measured by unpaired Student t test (for c) or one-way ANOVA with Tukey multiple comparison test (for e). BMBA, bone marrow—derived basophil; NS, not significant; OX, oxazolone; RNA-seq, RNA sequencing; scRNA-seq, single-cell RNA-seq.

#### **DISCUSSION**

Clinical studies reported that the topical treatment with PDE4 inhibitors effectively improve the disease severity and pruritus in patients with mild-to-moderate AD (Paller et al, 2016; Saeki et al, 2022a, 2022b), leading to the approval of crisaborole and difamilast for the treatment of AD. Nevertheless, the cellular and molecular mechanisms underlying their therapeutic effect on AD remain to be fully elucidated. In this study, we examined OX-induced skin allergic inflammation as a mouse model of AD and uncovered that difamilast

ameliorates skin inflammation through the suppression of IL-4 production by skin-infiltrating basophils.

PDE4 is the major family of PDE enzymes expressed in immune and inflammatory cells and composed of 4 subfamilies encoded by *Pde4a*, *Pde4b*, *Pde4c*, and *Pde4d*, respectively (Li et al, 2018; Maurice et al, 2014; Schick and Schlegel, 2022). The expression level of each subfamily varies depending on cell types and is differentially regulated by various inflammatory stimuli (Maurice et al, 2014). In this study, we demonstrated that mouse basophils display the

Il 4 expression of in basophils isolated on day 8 from the spleen and the OX-treated skin is shown. The value of Il 4 expression in spleen basophils from control-treated mice was set as 1. (mean  $\pm$  SEM, n = 4 mice each). (**f**-**h**)  $Mcpt8^{iCre}$   $Il 4^{fl}$  and control  $Mcpt8^{iCre}$  mice were treated with OX as in Figure 1. The mice were treated with difamilast or control ointment as in a. In **f**, the time course of  $\Delta$ Ear thickness is shown (mean  $\pm$  SEM, n = 3-4 mice each). In **g**, the H&E-stained specimens (Bars indicate 200 µm) on day 8 are shown. In **h**, the numbers of indicated cell types in the ear skin on day 8 are shown (mean  $\pm$  SEM, n = 3-4 mice each). Data shown in **b**-**h** are representative of at least three independent experiments. \* $^{*}P < .05$ , \* $^{**}P < .01$ , \* $^{**}P < .001$  measured by two-way ANOVA with Sidak multiple comparison test (for **b** and **f**) or with Tukey multiple comparison test (for **d**, **e**, and **h**). NS, not significant; OX, oxazolone; WT, wild-type.

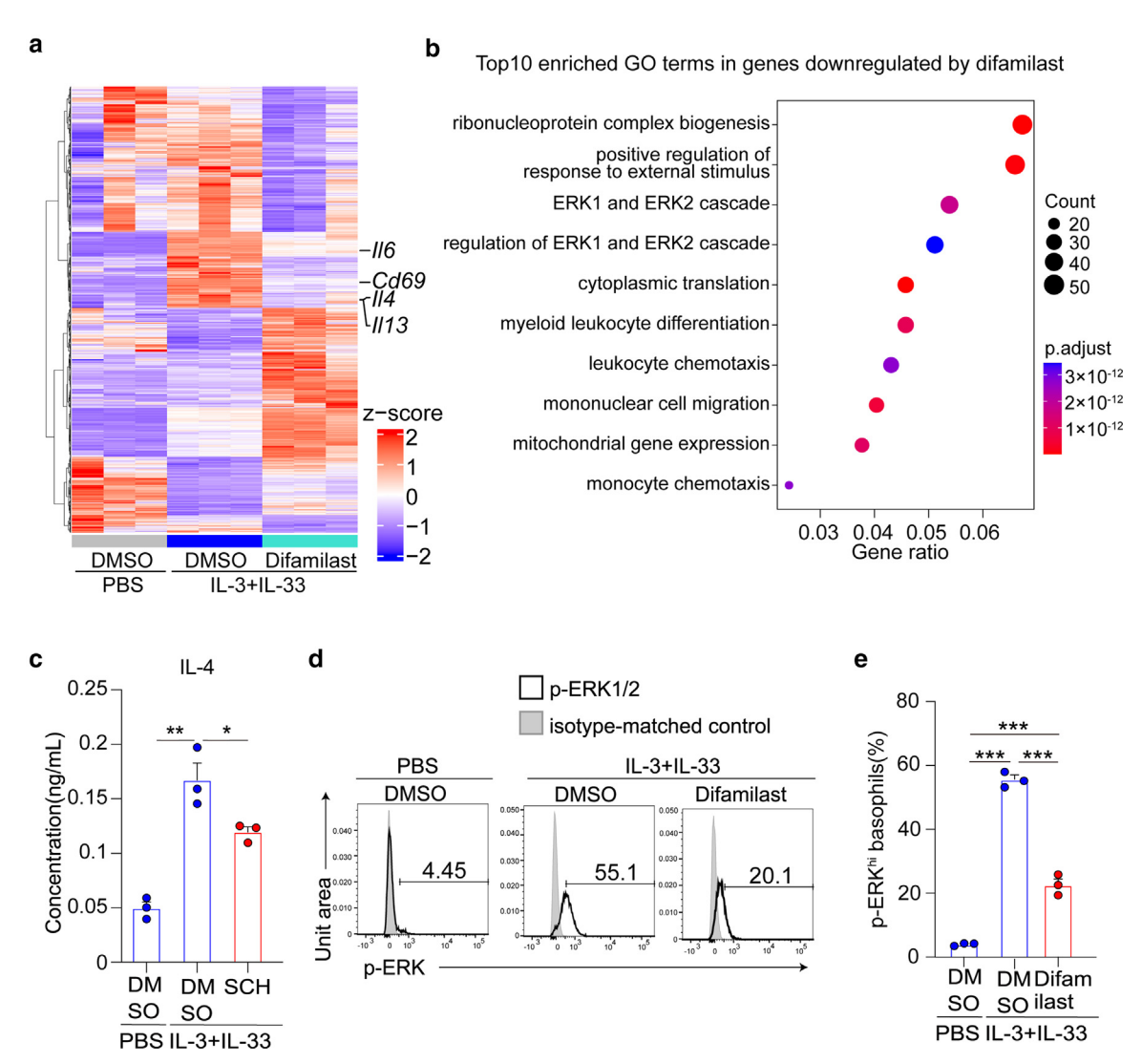


Figure 5. Difamilast blocks the ERK phosphorylation in activated basophils. BMBAs were generated as in Figure 4. ( $\bf a$  and  $\bf b$ ) BMBAs were stimulated by IL-3 + IL-33 or control PBS in the presence of difamilast (3  $\mu$ M) or vehicle DMSO alone for 4 hours and were subjected to bulk RNA-seq analysis (n=3, each). In  $\bf a$ , a hierarchically clustered heatmap of differentially expressed genes between difamilast- and vehicle-treated BMBAs is shown. In  $\bf b$ , the top 10 enriched GO terms in genes downregulated by difamilast are plotted in order of gene ratio. The size of the dots indicates the number of genes associated with indicated GO terms while the color of the dots indicates the adjusted P-values (P. adjust) calculated by one-sided Fisher's exact test with Benjamini-Hochberg correction. BMBAs were stimulated for 6 hours with IL-3 + IL-33 or control PBS in the presence of SCH772984 (SCH) or vehicle DMSO alone. IL-4 concentration in BMBA supernatants is shown (mean  $\pm$  SEM, n=3). ( $\bf d$  and  $\bf e$ ) BMBAs were stimulated by IL-3 + IL-33 or control PBS in the presence of difamilast (3  $\mu$ M) or vehicle DMSO alone for 10 minutes. In  $\bf d$ , the expression of phosphorylated ERK1/2 (p-ERK) in BMBAs is shown in open histograms. Shaded histograms indicate control staining with isotype-matched control. In  $\bf e$ , the frequency p-ERKhi cells is shown (mean  $\pm$  SEM, n=3). Data shown in  $\bf c-e$  are representative of at least three independent experiments. \*P < .05, \*\*\*P < .05, \*\*\*P < .001 measured by one-way ANOVA with Tukey multiple comparison test (for  $\bf c$  and  $\bf e$ ). GO, gene ontology.

highest expression of *Pde4b* among the PDE4 family at the resting state. Notably, the expression of *Pde4b*, but not other family members, was highly upregulated in basophils when stimulated in vitro with either cytokines or IgE/allergen, suggesting that the upregulated expression of *Pde4b* may be associated with the activation of basophils. In accordance with this, the treatment with difamilast, a potent and selective inhibitor of PDE4 especially the PDE4B, suppressed the IL-4 production by activated basophil in vitro. Transcriptomic analysis predicted that the difamilast treatment affected the expression of the genes associated with the ERK signaling cascade in cytokine-stimulated basophils. Indeed, the difamilast treatment decreased the phosphorylation of ERK

protein in parallel with the reduced production of IL-4 in cytokine-stimulated basophils. Thus, difamiliast appears to suppress the IL-4 production from basophils, at least in part, through inhibition of ERK phosphorylation.

The reanalysis of the publicly available single-cell RNA-seq data revealed that the Pde4b expression was upregulated in basophils accumulating in the skin lesion of the OX-induced AD model even though it remains to be determined what kind of factors promote the activation of basophils in the skin lesion. Taken together with the observation that the topical application of difamilast showed little therapeutic effect on the skin inflammation attenuated in  $II4^{-/-}$ , basophil-depleted or  $Mcpt8^{iCre}$   $II4^{fl}$  mice, it is likely that difamilast ameliorated

skin allergic inflammation by means of the suppression of IL-4 production through the inactivation of PDE4B in skin-infiltrating basophils. However, we cannot exclude the possibility that difamilast also affects cell types other than basophils.

We demonstrated in this study that the difamiliast treatment decreased the neutrophil infiltration concomitant with the reduced production of CXCL1 in the skin lesion of the OXinduced AD model. Mcpt8iCre 114fl mice showed reduced CXCL1 expression (Supplementary Figure S7a) and decreased neutrophil infiltration in the skin lesion, whereas the frequency of neutrophils in the peripheral blood under homeostatic condition was comparable between Mcpt8<sup>iCre</sup> II4<sup>fl</sup> and control mice (Supplementary Figure S7b). Therefore, basophil-derived IL-4 appears to stimulate CXCL1 production in the skin, leading to the enhanced recruitment of neutrophils to the skin in this model, despite the previous report showing that IL-4 rather suppresses the recruitment of neutrophil to the skin in bacterial infection models (Woytschak et al, 2016). Providing that neutrophils are reported to promote skin inflammation in OX-induced skin inflammation models (Lv et al, 2015; Strzepa et al, 2020; Weber et al, 2015), one may assume that basophil-derived IL-4 promotes skin inflammation partly through facilitating neutrophil recruitment to the skin lesion in this model.

Re-analysis of the single-cell RNA-seq datasets (Liu et al, 2020) (Supplementary Figure S4a) revealed that Cxcl1 is predominantly expressed in fibroblasts in the OX-induced AD-like skin lesion (Supplementary Figure S4b). Moreover, ligand-receptor interactome analysis inferred the intimate interactions between basophils and fibroblasts via IL-4 signaling (Supplementary Figure S4c). Accordingly, it is assumed that IL-4 secreted by skin-infiltrating basophils may act on skin fibroblasts to produced CXCL1, promoting neutrophil recruitment. Alternatively, it can also be assumed that IL-4 promotes an itch response (Oetjen et al, 2017) that damages skin to promote CXCL1 production and neutrophil recruitment to the skin (Walsh et al, 2019). Difamilast might block these cascades and therefore decreases the infiltration of neutrophils to the skin lesion. Notably, in an ovalbumininduced AD model, the topical application of crisaborole ointment has been shown to decrease the levels of neutrophil attracting chemokines in the skin lesion, leading to the reduced neutrophil infiltration and suppression of itch sensation (Sakai et al, 2021). Given that skin-infiltrating basophils are the major producers of IL-4 in the ovalbumininduced AD model (Leyva-Castillo et al, 2022), crisaborole perhaps acts on skin-infiltrating basophils to suppress the neutrophil infiltration in a way similar to that observed in the OX-induced AD model mice. Because the treatment of patients with AD with crisaborole ointment reportedly suppresses the expression of neutrophil attracting chemokines (CXCL1, CXCL2, and CXCL8) in the skin lesion (Bissonnette et al, 2019), it is possible that the common mechanism is operative in the AD mouse models and patients with AD, namely PDE4 inhibitor-mediated suppression of neutrophil accumulation in the skin lesion.

In conclusion, this study demonstrated that difamilast ameliorates skin inflammation in the OX-induced AD model by the suppression of basophil IL-4 production, most likely through inhibition of ERK phosphorylation in basophils. Providing that the accumulation of basophils can be detected in more than half of patients with AD (Ito et al, 2011; Kim et al, 2014; Mashiko et al, 2017), PDE4 inhibitors including difamilast might show the therapeutic effect on AD inflammation, at least in part, through suppression of basophil activation, particularly in patients with AD with basophil infiltration in the skin lesion.

#### **MATERIALS AND METHODS**

#### Mice

C57BL/6J mice were purchased from Sankyo Labo Service Corporation. *Mcpt8*<sup>DTR/+</sup> knock-in mice (Wada et al, 2010), *II4*<sup>-/-</sup> mice (Kopf et al, 1993), *Mcpt8*<sup>iCre</sup> and *Mcpt8*<sup>iCre</sup> *II4*<sup>fl</sup> mice (Shibata et al, 2018) were described previously. All mice were maintained under specific pathogen-free conditions in our animal facilities. All animal experiments were approved by the Institutional Animal Care and Use Committee of Tokyo Medical and Dental University (A2022-023C)

#### OX-induced murine skin inflammation model

OX-induced AD-like skin inflammation model was induced as described previously (Yamanishi et al., 2020). In brief, mice were first epicutaneously sensitized with 100 µl of 3% OX (MilliporeSigma) on their abdomen 7 days before the first challenge, and repeatedly challenged every other day with topical application of 10 µl of 0.5% OX and vehicle alone on their right and left ear, respectively. For ointment application, 30 µg per ear of 1% difamilast ointment (Otsuka Pharmaceuticals) or ointment base alone were applied to both their right and left ears, 30 minutes after the challenge of 0.5% OX. For the antibody-mediated basophil depletion, mice were intravenously injected with 50 µg of anti-CD200R3 monoclonal antibody (clone: Ba160; prepared from hybridoma in our laboratory) or its isotypematched control antibody (clone: RTK4530; BioLegend) 1 day before and 4 and 7 days after the first OX challenge. For the diphtheria toxin-mediated basophil depletion, Mcpt8<sup>DTR/+</sup> mice were intravenously injected with 500 ng of diphtheria toxin (MilliporeSigma) or its inactive mutant (Glu<sup>52</sup>)-diphtheria toxin (MilliporeSigma) 1 day before and 4 and 7 days after the first OX challenge. For H&E staining, ear specimens were fixed for 18 hours with 4% paraformaldehyde/ PBS solution, embedded in paraffin, cut into 5 µm-thick sections, and stained with H&E (Muto pure chemicals).

#### Flow cytometric analysis and cell sorting

The ear was incubated in complete RPMI (RPMI 1640 medium [Nacalai tesque] supplemented with 10% fetal bovine serum [MilliporeSigma], 1 mM sodium pyruvate [Nacalai tesque], 0.055 mM 2-mercaptoethanol [Thermo Fisher Scientific], 100 units/ml penicillin/streptomycin [Nacalai tesque], and 0.1 mM MEM nonessential amino acids solution [Nacalai tesque]) containing 150 units/ ml of collagenase (FUJIFILM Wako Pure Chemical) for 2 hours. Cells were then treated by normal rat serum (MilliporeSigma) and 2.5 μg/ ml of TruStain FcX PLUS antibody (BioLegend), followed by staining with the indicated antibodies on ice for 20 minutes, and analyzed by FACSLyric (BD Biosciences) and FlowJo ver.10.8.2 (BD Biosciences) or sorted by FACSAriaIII (BD Biosciences). Dead cells were excluded by staining with 1 µg/ml of propidium iodide (MilliporeSigma). Cell lineages were defined as follows: hematopoietic cell (CD45<sup>+</sup>), neutrophil (CD45<sup>+</sup>Ly6G<sup>+</sup>), macrophage (CD45<sup>+</sup>SiglecF<sup>-</sup>Ly6G<sup>-</sup> CD11b<sup>+</sup>F4/80<sup>+</sup>), eosinophil (CD45<sup>+</sup>SiglecF<sup>+</sup>), and basophil (CD45<sup>+</sup>c-Kit<sup>-</sup>CD49b<sup>+</sup>CD200R3<sup>+</sup>).

Inhibitory Effect of Difamilast on Basophils

#### The generation and stimulation of BMBAs

BMBAs were generated by culturing bone marrow cells in complete RPMI containing 0.3 ng/ml of recombinant mouse IL-3 (BioLegend) for 7 days, followed by magnetic sorting of CD49b<sup>+</sup> cells by using biotinylated anti-CD49b antibody (clone: DX5; BioLegend) and Mojosort streptavidin nanoparticles (BioLegend). For antigen/IgE stimulation, they were sensitized with 2,4,6-trinitrophenol-specific IgE (1 μg/ml) for 18 hours and then incubated at 37 °C with 2,4,6trinitrophenol-conjugated ovalbumin or control ovalbumin (10 ng/ ml) for 1 hour in the surface CD63 expression assay, for 4 hours in the transcriptomic analyses or for 6 hours in the IL-4 production assay. For non-IgE stimulation, nonsensitized BMBAs were incubated at 37 °C with IL-3 (10 ng/ml) plus IL-33 (10 ng/ml; BioLegend) or PBS for 4 hours in transcriptomic analyses or for 6 hours in the IL-4 production assay. IL-4 concentration in culture supernatants was measured by ELISA MAX standard (BioLegend). For PDE inhibition, difamilast (Otsuka Pharmaceuticals), GEBR-7b (MilliporeSigma), or DMSO were added to the culture medium just before the addition of indicated stimulants. For cell viability assay, BMBAs stained by acridine orange and DAPI (solution 18; ChemoMetec) were analyzed by NucleoCounter NC-250 (ChemoMetec). For detection of phosphorylated ERK, BMBAs stimulated for 10 minutes with IL-3 + IL-33 were fixed by 4% paraformaldehyde/PBS solution, stained with cell surface molecules, permeabilized by True-Phos Perm Buffer (Bio-Legend), and stained with anti-phosphorylated ERK or its isotypematched control antibody.

#### Bulk RNA-seq analysis and other transcriptomic analyses

Bulk RNA-seq analysis of BMBAs were performed as described previously (Miyake et al, 2023; Ogawa et al, 2022). The detailed methods for qRT-PCR analysis, bulk RNA-seq analysis, reanalysis of single-cell RNA-seq data and statistical analysis are described in Supplementary Materials and Methods.

#### **DATA AVAILABILITY STATEMENT**

Transcriptomic data generated in this study have been deposited in NCBI Gene expression omnibus (GEO) under accession number GSE234541 (https://www.ncbi.nlm.nih.gov/geo/query/acc.cgi?acc=GSE234541).

#### ORCID

Kazufusa Takahashi: https://orcid.org/0009-0007-9407-7111
Kensuke Miyake: https://orcid.org/0000-0003-1149-3755
Junya Ito: https://orcid.org/0009-0000-0239-3969
Hinano Shimamura: https://orcid.org/0009-0006-0295-6585
Tadahiro Suenaga: https://orcid.org/0009-0006-6802-4844
Hajime Karasuyama: https://orcid.org/0000-0003-0689-0836
Kenichi Ohashi: https://orcid.org/0000-0003-1836-1763

#### **CONFLICT OF INTEREST**

Part of this work was sponsored and funded by Otsuka Pharmaceutical Co, Ltd  $\,$ 

#### **ACKNOWLEDGMENTS**

This work was supported by research funding from Otsuka Pharmaceutical Co, Ltd and research grants from the Japanese Ministry of Education, Culture, Sports, Science, and Technology (22K007115 [KM], 19H01025 [HK], 22H02845 [HK]), Takeda Science Foundation (KM), KANAE Foundation for the Promotion of Medical Science (KM), The Uehara Memorial Foundation (KM), The Naito Foundation (KM), Ohyama Health Foundation (KM), and JST SPRING, Grant Number JPMJSP2120 (JI and KT). We thank ImmunoGeneTeqs, Inc. for support of bulk RNA-seq analysis; K. Mogi, M. Suda and T. Kojma for technical support; all the members of the Karasuyama laboratory for helpful discussions; and A. Furukawa and M. Kinoshita for secretary assistance. Cell sorting by using FACS AriallI was performed in part at Research Core of Tokyo Medical and Dental University (TMDU).

#### **AUTHOR CONTRIUTIONS**

Conceptualization: KT, KM, HK; Funding Acquisition: KT, KM, HK; Investigation: KT, KM, HS; Formal analysis: KT, KM, JI; Supervision: KM, HK, KO; Writing — Original Draft Preparation: KT, KM, HK; Writing — Review and Editing: KT, KM, JI, HS, TS, HK, KO

#### **SUPPLEMENTARY MATERIAL**

Supplementary material is linked to the online version of the paper at www. jidonline.org, and at https://doi.org/10.1016/j.jid.2023.09.272.

#### **REFERENCES**

- Bissonnette R, Pavel AB, Diaz A, Werth JL, Zang C, Vranic I, et al. Crisaborole and atopic dermatitis skin biomarkers: an intrapatient randomized trial. J Allergy Clin Immunol 2019;144:1274—89.
- Calverley PM, Sanchez-Toril F, McIvor A, Teichmann P, Bredenbroeker D, Fabbri LM. Effect of 1-year treatment with Roflumilast in severe chronic obstructive pulmonary disease. Am J Respir Crit Care Med 2007;176: 154–61
- Chen HF, Chuang HC, Tan TH. Regulation of dual-specificity phosphatase (DUSP) ubiquitination and protein stability. Int J Mol Sci 2019;20.
- Fabbri LM, Calverley PM, Izquierdo-Alonso JL, Bundschuh DS, Brose M, Martinez FJ, et al. Roflumilast in moderate-to-severe chronic obstructive pulmonary disease treated with longacting bronchodilators: two randomised clinical trials. Lancet 2009;374:695—703.
- Guttman-Yassky E, Hanifin JM, Boguniewicz M, Wollenberg A, Bissonnette R, Purohit V, et al. The role of phosphodiesterase 4 in the pathophysiology of atopic dermatitis and the perspective for its inhibition. Exp Dermatol 2019;28:3–10.
- Hiyama H, Arichika N, Okada M, Koyama N, Tahara T, Haruta J. Pharmacological profile of difamilast, a novel selective phosphodiesterase 4 inhibitor, for the topical treatment of atopic dermatitis. J Pharmacol Exp Ther 2023;386:45–55.
- Ito Y, Satoh T, Takayama K, Miyagishi C, Walls AF, Yokozeki H. Basophil recruitment and activation in inflammatory skin diseases. Allergy 2011;66: 1107–13.
- Jin SL, Goya S, Nakae S, Wang D, Bruss M, Hou C, et al. Phosphodiesterase 4B is essential for T(H)2-cell function and development of airway hyperresponsiveness in allergic asthma. J Allergy Clin Immunol 2010;126: 1252–9.e12.
- Kim BS, Wang K, Siracusa MC, Saenz SA, Brestoff JR, Monticelli LA, et al. Basophils promote innate lymphoid cell responses in inflamed skin. J Immunol 2014;193:3717–25.
- Kleinman E, Laborada J, Metterle L, Eichenfield LF. What's new in topicals for atopic dermatitis? Am J Clin Dermatol 2022;23:595–603.
- Kopf M, Le Gros G, Bachmann M, Lamers MC, Bluethmann H, Köhler G. Disruption of the murine IL-4 gene blocks Th2 cytokine responses. Nature 1993;362:245—8.
- Leyva-Castillo JM, Sun L, Wu SY, Rockowitz S, Sliz P, Geha RS. Single-cell transcriptome profile of mouse skin undergoing antigen-driven allergic inflammation recapitulates findings in atopic dermatitis skin lesions. J Allergy Clin Immunol 2022;150:373–84.
- Li H, Zuo J, Tang W. Phosphodiesterase-4 inhibitors for the treatment of inflammatory diseases. Front Pharmacol 2018;9:1048.
- Liu Y, Cook C, Sedgewick AJ, Zhang S, Fassett MS, Ricardo-Gonzalez RR, et al. Single-cell profiling reveals divergent, globally patterned immune responses in murine skin inflammation. iScience 2020;23:101582.
- Lv J, Zou L, Zhao L, Yang W, Xiong Y, Li B, et al. Leukotriene B(4)-leukotriene B(4) receptor axis promotes oxazolone-induced contact dermatitis by directing skin homing of neutrophils and CD8(+) T cells. Immunology 2015:146:50–8
- Mashiko S, Mehta H, Bissonnette R, Sarfati M. Increased frequencies of basophils, type 2 innate lymphoid cells and Th2 cells in skin of patients with atopic dermatitis but not psoriasis. J Dermatol Sci 2017;88:167–74.
- Maurice DH, Ke H, Ahmad F, Wang Y, Chung J, Manganiello VC. Advances in targeting cyclic nucleotide phosphodiesterases. Nat Rev Drug Discov 2014;13:290–314.
- Miyake K, Ito J, Nakabayashi J, Shichino S, Ishiwata K, Karasuyama H. Single cell transcriptomics clarifies the basophil differentiation trajectory and identifies pre-basophils upstream of mature basophils. Nat Commun 2023;14:2694.

- Nakagawa H, Nemoto O, Igarashi A, Saeki H, Kaino H, Nagata T. Delgocitinib ointment, a topical Janus kinase inhibitor, in adult patients with moderate to severe atopic dermatitis: a phase 3, randomized, double-blind, vehicle-controlled study and an open-label, long-term extension study. J Am Acad Dermatol 2020;82:823—31.
- Oetjen LK, Mack MR, Feng J, Whelan TM, Niu H, Guo CJ, et al. Sensory neurons co-opt classical immune signaling pathways to mediate chronic itch. Cell 2017;171:217–28.e13.
- Ogawa T, Shichino S, Ueha S, Ogawa S, Matsushima K. Complement protein C1q activates lung fibroblasts and exacerbates silica-induced pulmonary fibrosis in mice. Biochem Biophys Res Commun 2022;603:88–93.
- Paller AS, Tom WL, Lebwohl MG, Blumenthal RL, Boguniewicz M, Call RS, et al. Efficacy and safety of crisaborole ointment, a novel, nonsteroidal phosphodiesterase 4 (PDE4) inhibitor for the topical treatment of atopic dermatitis (AD) in children and adults. J Am Acad Dermatol 2016;75: 494–503.e6.
- Papp K, Reich K, Leonardi CL, Kircik L, Chimenti S, Langley RG, et al. Apremilast, an oral phosphodiesterase 4 (PDE4) inhibitor, in patients with moderate to severe plaque psoriasis: results of a phase III, randomized, controlled trial (Efficacy and Safety Trial Evaluating the Effects of apremilast in Psoriasis [ESTEEM] 1). J Am Acad Dermatol 2015;73:37–49.
- Robichaud A, Stamatiou PB, Jin SL, Lachance N, MacDonald D, Laliberté F, et al. Deletion of phosphodiesterase 4D in mice shortens alpha(2)-adrenoceptor-mediated anesthesia, a behavioral correlate of emesis. J Clin Invest 2002;110:1045–52.
- Saeki H, Baba N, Ito K, Yokota D, Tsubouchi H. Difamilast, a selective phosphodiesterase 4 inhibitor, ointment in paediatric patients with atopic dermatitis: a phase III randomized double-blind, vehicle-controlled trial. Br J Dermatol 2022a;186:40–9.
- Saeki H, Ito K, Yokota D, Tsubouchi H. Difamilast ointment in adult patients with atopic dermatitis: a phase 3 randomized, double-blind, vehicle-controlled trial. J Am Acad Dermatol 2022b;86:607—14.
- Sakai K, Sanders KM, Pavlenko D, Lozada T, Akiyama T. Crisaborole prevents infiltration of neutrophils to suppress itch in a mouse model of atopic dermatitis. Itch 2021;6:e53.
- Schick MA, Schlegel N. Clinical implication of Phosphodiesterase-4-Inhibition. Int J Mol Sci 2022;23.
- Shibata S, Miyake K, Tateishi T, Yoshikawa S, Yamanishi Y, Miyazaki Y, et al. Basophils trigger emphysema development in a murine model of COPD through IL-4-mediated generation of MMP-12-producing macrophages. Proc Natl Acad Sci U S A 2018;115:13057—62.

- Simpson EL, Bieber T, Guttman-Yassky E, Beck LA, Blauvelt A, Cork MJ, et al. Two Phase 3 Trials of Dupilumab versus Placebo in Atopic Dermatitis. N Engl J Med 2016;375:2335–48.
- Strzepa A, Gurski CJ, Dittel LJ, Szczepanik M, Pritchard KA Jr, Dittel BN. Neutrophil-derived myeloperoxidase facilitates both the induction and elicitation phases of contact hypersensitivity. Front Immunol 2020;11: 608871
- Tavares LP, Negreiros-Lima GL, Lima KM, PMR ES, Pinho V, Teixeira MM, et al. Blame the signaling: role of cAMP for the resolution of inflammation. Pharmacol Res 2020;159:105030.
- Thyssen JP, Vestergaard C, Deleuran M, de Bruin-Weller MS, Bieber T, Taieb A, et al. European Task Force on Atopic Dermatitis (ETFAD): treatment targets and treatable traits in atopic dermatitis. J Eur Acad Dermatol Venereol 2020;34:e839–42.
- Wada T, Ishiwata K, Koseki H, Ishikura T, Ugajin T, Ohnuma N, et al. Selective ablation of basophils in mice reveals their nonredundant role in acquired immunity against ticks. J Clin Invest 2010;120: 2867–75.
- Walsh CM, Hill RZ, Schwendinger-Schreck J, Deguine J, Brock EC, Kucirek N, et al. Neutrophils promote CXCR3-dependent itch in the development of atopic dermatitis. eLife 2019;8.
- Weber FC, Németh T, Csepregi JZ, Dudeck A, Roers A, Ozsvári B, et al. Neutrophils are required for both the sensitization and elicitation phase of contact hypersensitivity. J Exp Med 2015;212:15—22.
- Weidinger S, Beck LA, Bieber T, Kabashima K, Irvine AD. Atopic dermatitis. Nat Rev Dis Primers 2018;4:1.
- Weidinger S, Novak N. Atopic dermatitis. Lancet 2016;387:1109-22.
- Woytschak J, Keller N, Krieg C, Impellizzieri D, Thompson RW, Wynn TA, et al. Type 2 interleukin-4 receptor signaling in neutrophils antagonizes their expansion and migration during infection and inflammation. Immunity 2016;45:172–84.
- Yamanishi Y, Mogi K, Takahashi K, Miyake K, Yoshikawa S, Karasuyama H. Skin-infiltrating basophils promote atopic dermatitis-like inflammation via IL-4 production in mice. Allergy 2020;75:2613–22.

© (1) S (2)

This work is licensed under a Creative Commons Attribution-NonCommercial-NoDerivatives 4.0

International License. To view a copy of this license, visit http://creativecommons.org/licenses/by-nc-nd/4.0/

#### SUPPLEMENTARY MATERIALS AND METHODS

#### **Antibodies and reagents**

The following antibodies were purchased from BioLegend: APC-conjugated anti-CD200R3 (Ba13), APC-Cy7-conjugated anti-Ly6G (1A8), Brilliant Violet 421-conjugated CD11b (M1/ 70), FITC-conjugated anti-CD45 (30-F11), Pacific Blueconjugated anti-c-Kit (2B8), PE-conjugated anti-CD63 (NVG-2), anti-IL-3Rα (5B11), anti-CD45 (30-F11), anti-FcεRIα (MAR-1), anti-IL-33R (DIH9), Armenian hamster IgG isotype control (HTK888) and rat IgG2a κ isotype control (RTK2758), PE-Cy7-conjugated anti-CD49b (HMα2) and anti-F4/80 (BM8). Alexa Fluor 647-conjugated anti-Siglec-F (E50-2440), anti-phosphorylated ERK1/2 (20A), and mouse IgG1 κ isotype control (MOPC-21) were purchased from BD Biosciences. TNP-specific IgE antibody (clone: IGEL-b4; ATCC) and anti-CD200R3 antibody (clone: Ba160) were prepared from hybridoma in our laboratory. Oxazolone (4-Ethoxymethylene-2-phenyl-2-oxazolin-5-one) and GEBR-7b were purchased from MilliporeSigma. SCH772984 was purchased from Selleck chemicals. Bulk powder of difamilast, 1% difamilast ointment and ointment base were provided from Otsuka Pharmaceutical Co, Ltd.

#### Measurement of cytokines and chemokine in the skin lesions

The ear skins suspended in T-PER tissue protein extraction reagent (Thermo Fisher Scientific) supplemented with Halt protease and phosphatase inhibitor cocktail (Thermo Fisher Scientific) were homogenized by using zirconium oxide beads and Precellys evolution (Bertin Technologies). The amounts of cytokines and chemokines in ear homogenate were measured by LEGENDplex Multiplex Assay (Bio-Legend), according to the manufacturer's protocol.

#### qRT-PCR

For qRT-PCR of sort-purified basophils, cDNA was synthesized from 300 cells of basophils by using QuantAccuracy, RT-RamDA cDNA synthesis kit (TOYOBO), according to the manufacturer's protocol. For qRT-PCR of marrow-derived basophils, total RNA was extracted by RNeasy Mini Kit (Qiagen), followed by cDNA synthesis with SuperScript IV VILO master mix (Thermo Fisher Scientific). qRT-PCR of cDNAs was performed on StepOnePlus Real-Time PCR system (Thermo Fisher Scientific) by using Fast SYBR Green master mix (Thermo Fisher Scientific) and following primer sets: 5'-GGCATTTTGAACGAGGTCAC-3' and 5'-AAATATGCGAAGCACCTTGG-3' for Il4, 5'-AAAA GCTGGTACACCCGGAA-3' and 5'-TTCAGTAAGTCCCGCT CCTGG-3' for Pde4a, 5'-CTGACCGGATACAGGTTCTTCG-3' and 5'-CTCCCACAGTGGATGGACAA-3' for Pde4b, 5'-GGAGTTCTTTAGACAGGGTGACA-3' and 5'-CAGTCTGG-GAGCTTTCGTCA-3' for Pde4c, 5'-TGCTCTCTACACCC GCTTTG-3' and 5'-AGAGCGAGTTCCGAGTTTGT-3' for Pde4d, and 5'-GCCCCTGCACTCTCGCTTTC-3' and 5'-TGCC AGGACGCGCTTGT-3' for *Rplp0*. Relative gene expression levels were calculated by  $\Delta\Delta$ CT method with normalization using Rplp0 expression.

#### **Bulk RNA sequencing analysis**

Bulk RNA sequencing analysis of bone marrow-derived basophils were performed as described previously (Miyake et al, 2023; Ogawa et al, 2022). Ten thousand cells of bone marrow-derived basophils were lysed by using lithium dodecyl sulfate-based lysis buffer and mRNA was isolated by using Dynabeads M-270 conjugated with oligo dT. On-beads reverse transcription was performed by SuperScript IV reverse transcriptase (Thermo Fisher Scientific), and polyCtailing, second strand synthesis, and whole-transcriptome amplification was performed by TAS-Seq workflow (Shichino et al, 2022). Whole-transcriptome library was subjected to fragmentation/end-repair/A-tailing using NEBNext Ultra II FS DNA Library Prep Kit for Illumina (New England Biolabs). Pooled libraries were sequenced by Illumina Novaseg 6000 sequencer (Illumina). After adapter trimming by using Cutadapt-v3.4 (Martin, 2011), the filtered reads were mapped to reference RNA (GRCm38 release-101) using Bowtie2-2.4.2 (Langmead and Salzberg, 2012) and read number of each gene were counted. Data normalization and differential expression analyses were performed by TCC v.1.38.0 (Sun et al, 2013) in R 4.2.3. GO enrichment analysis and heatmap visualization were performed by clusterProfiler v4.6.2 and Complex-Heatmap v2.14.0, respectively (Gu, 2022; Wu et al, 2021).

#### Re-analysis of single-cell RNA sequencing data

Re-analysis of single-cell RNA sequencing data of the skin lesion of oxazolone-induced mouse AD model deposited in NCBI GEO (accession number: GSE149121) (Liu et al, 2020) was analyzed using R software package Seurat v4.3.0 (Hao et al, 2021) in R 4.2.3. As quality control, cells with the mitochondrial gene proportion >25% were filtered out. The log-normalized gene counts were calculated using NormalizeData function and highly variable genes were defined by FindVariableFeatures function. Principal component analysis was performed on the variable genes, and principal components with their P-value < .05 calculated by the jackstraw method, were subjected to cell clustering and dimensional reduction using Uniform Manifold Approximation and Projection. Then, we re-clustered GSE14921 excluding human cells and Uniform Manifold Approximation and Projection dimensional reduction was conducted (resolution = 1.0). Ligand-receptor interaction network analysis was performed by CellChat v1.6.1 (Jin et al, 2021).

#### Statistical analysis

The analysis between two groups was performed with unpaired Student's t test. Analysis between more than three groups was performed with one-way or two-way ANOVA. All statistical analyses were performed by using GraphPad PRISM ver.9.5.0 (GraphPad Software). P-value < .05 was considered statistically significant.

#### **SUPPLEMENTARY REFERENCES**

Gu Z. Complex heatmap visualization. iMeta 2022;1:e43.

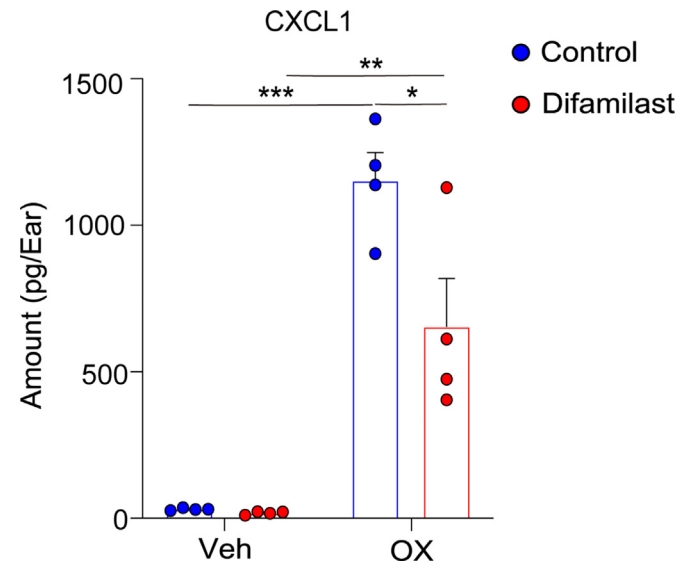
Hao Y, Hao S, Andersen-Nissen E, Mauck WM 3rd, Zheng S, Butler A, et al. Integrated analysis of multimodal single-cell data. Cell 2021;184: 3573-87.e29.

Jin S, Guerrero-Juarez CF, Zhang L, Chang I, Ramos R, Kuan CH, et al. Inference and analysis of cell-cell communication using CellChat. Nat Commun 2021;12:1088.

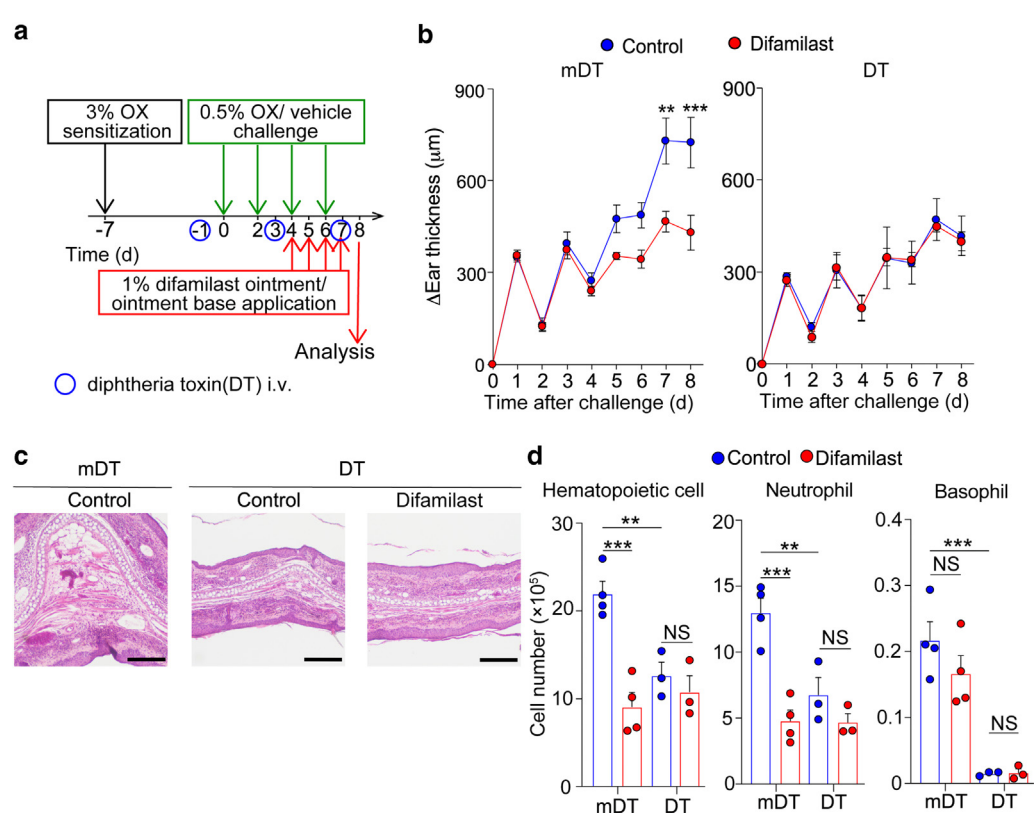
Langmead B, Salzberg SL. Fast gapped-read alignment with Bowtie 2. Nat Methods 2012;9:357-9.

Liu Y, Cook C, Sedgewick AJ, Zhang S, Fassett MS, Ricardo-Gonzalez RR, et al. Single-cell profiling reveals divergent, globally patterned immune responses in murine skin inflammation. iScience 2020;23:101582.

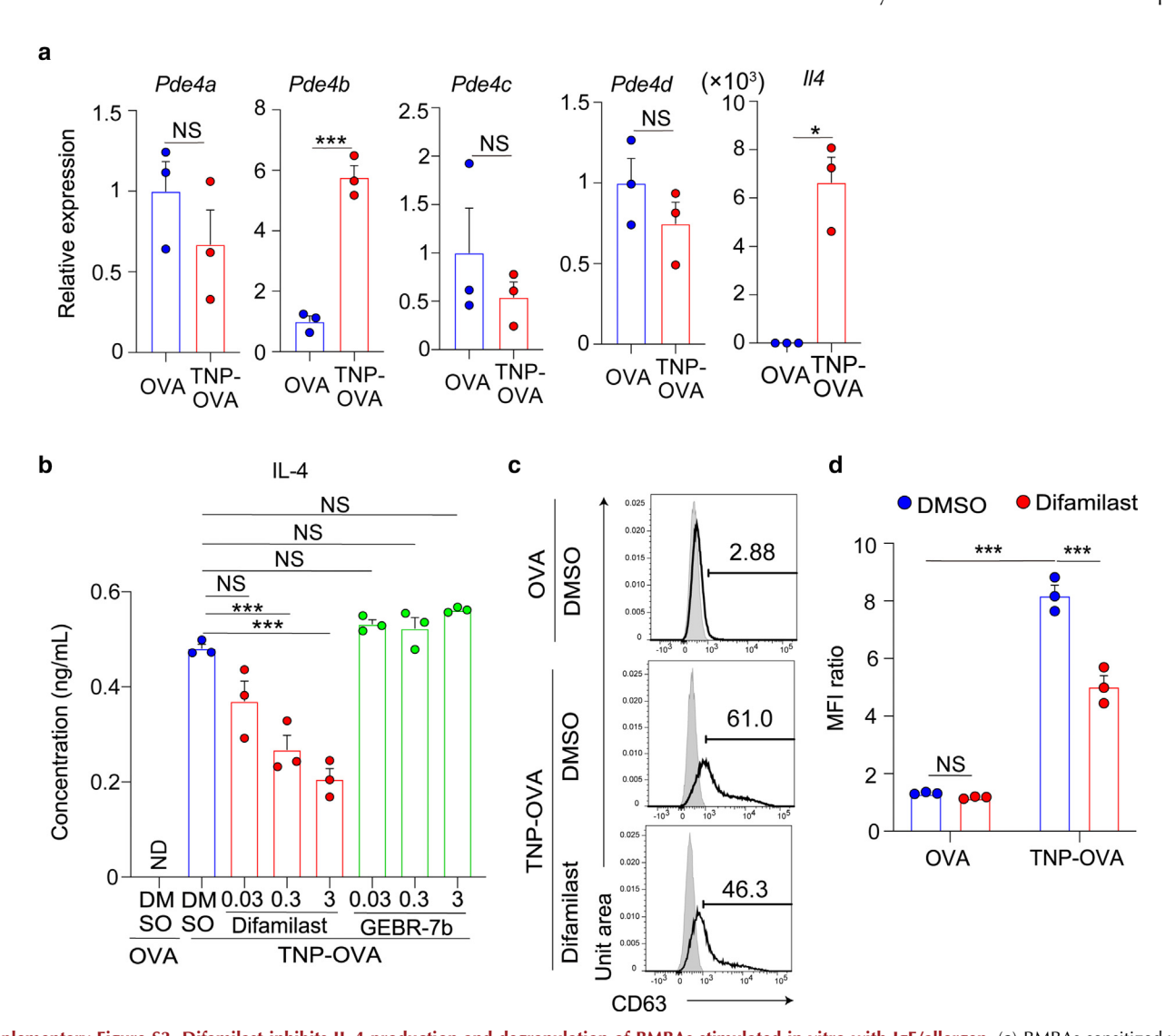
- Martin M. Cutadapt removes adapter sequences from high-throughput sequencing reads. EMBnet j 2011;17.
- Miyake K, Ito J, Nakabayashi J, Shichino S, Ishiwata K, Karasuyama H. Single cell transcriptomics clarifies the basophil differentiation trajectory and identifies pre-basophils upstream of mature basophils. Nat Commun 2023;14:2694.
- Ogawa T, Shichino S, Ueha S, Ogawa S, Matsushima K. Complement protein C1q activates lung fibroblasts and exacerbates silica-induced pulmonary fibrosis in mice. Biochem Biophys Res Commun 2022;603:88-93.
- Shichino S, Ueha S, Hashimoto S, Ogawa T, Aoki H, Wu B, et al. TAS-Seq is a robust and sensitive amplification method for bead-based scRNA-seq. Commun Biol 2022;5:602.
- Sun J, Nishiyama T, Shimizu K, Kadota K. TCC: an R package for comparing tag count data with robust normalization strategies. BMC Bioinformatics 2013;14:219.
- Wu T, Hu E, Xu S, Chen M, Guo P, Dai Z, et al. clusterProfiler 4.0: a universal enrichment tool for interpreting omics data. Innovation (Camb) 2021;2:



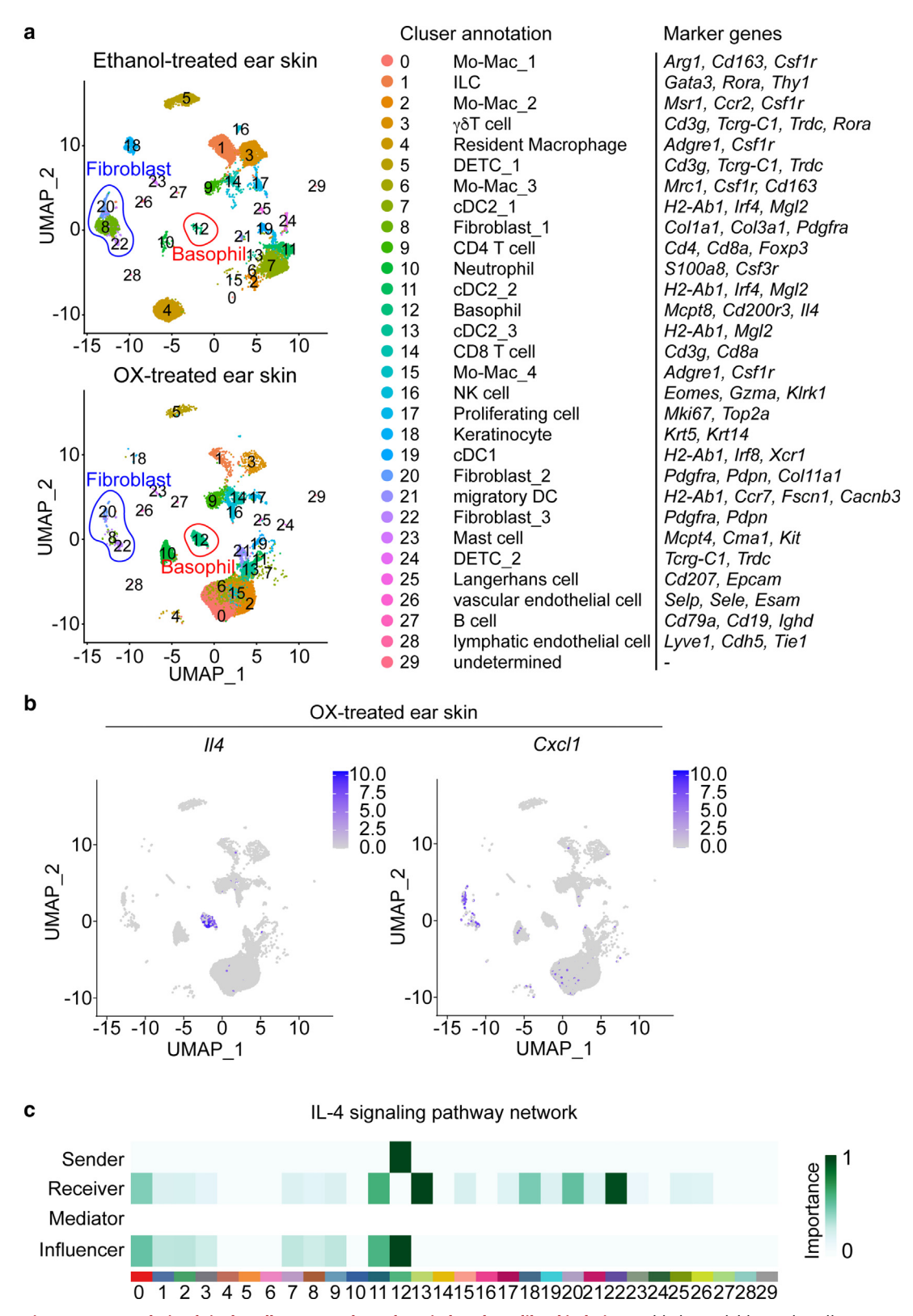
Supplementary Figure S1. Difamilast treatment reduces the amount of CXCL1 in the OX-treated skin. C57BL/6 mice were treated with OX as in Figure 1. Difamilast or control ointment was applied daily to their ear skin starting after the third OX challenge. The amounts of CXCL1 in tissue homogenates collected from OX-induced skin lesion are shown (mean  $\pm$ SEM, n = 4 mice each). \*P < .05, \*\*P < .01, \*\*\*P < .001 measured by twoway ANOVA with Tukey multiple comparison test. OX, oxazolone; Veh, vehicle.



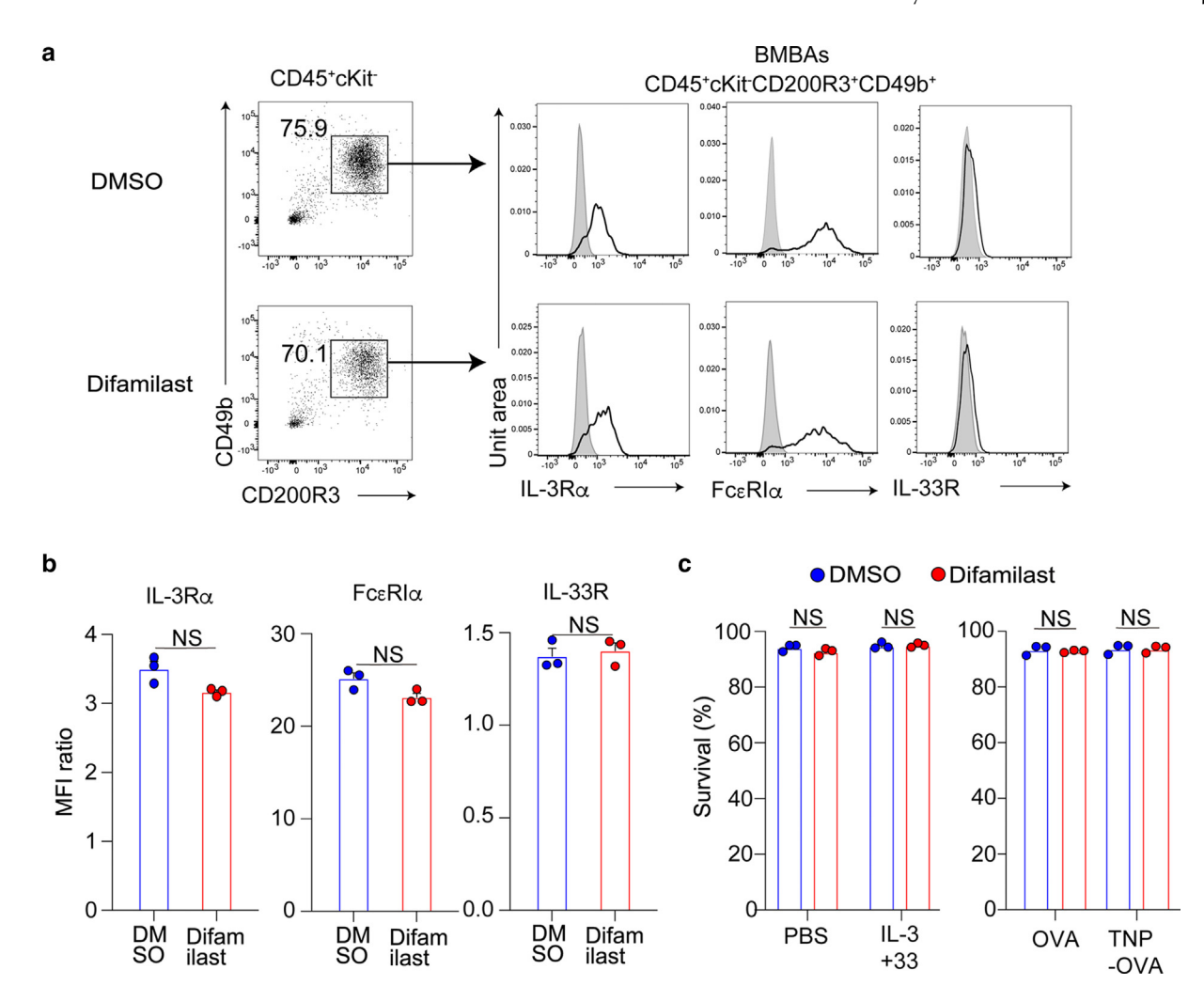
Supplementary Figure S2. Difamilast shows little or no further therapeutic effect on the attenuated skin inflammation in basophil-depleted  $Mcpt8^{DTR/+}$  mice.  $Mcpt8^{DTR/+}$  knock-in mice were treated with OX as in Figure 1. Difamilast or control ointment was applied daily to their ear skin, starting after the third OX challenge. Diphtheria toxin (DT) or its inactive mutant (mutant DT; mDT) was intravenously administered to mice on 1 day before, 4 and 7 days after the first OX challenge (as indicated by blue circles in a). (a) The experimental protocol is depicted. (b) The time course of  $\Delta$ Ear thickness is shown (mean  $\pm$  SEM, n = 3 mice each). (c) The H&E-stained specimens (Bars indicate 200  $\mu$ m) on day 8 are shown. (d) The numbers of indicated cell types in the ear skin on day 8 are shown (mean  $\pm$  SEM, n = 3-4 mice each). Data shown in b-d are representative of at least three independent experiments. \*\*P < .01, \*\*\*P < .001 measured by two-way ANOVA with Sidak multiple comparison test (for b) or with Tukey multiple comparison test (for e). DT, diphtheria toxin; mDT, mutant DT; NS, not significant; OX, oxazolone.



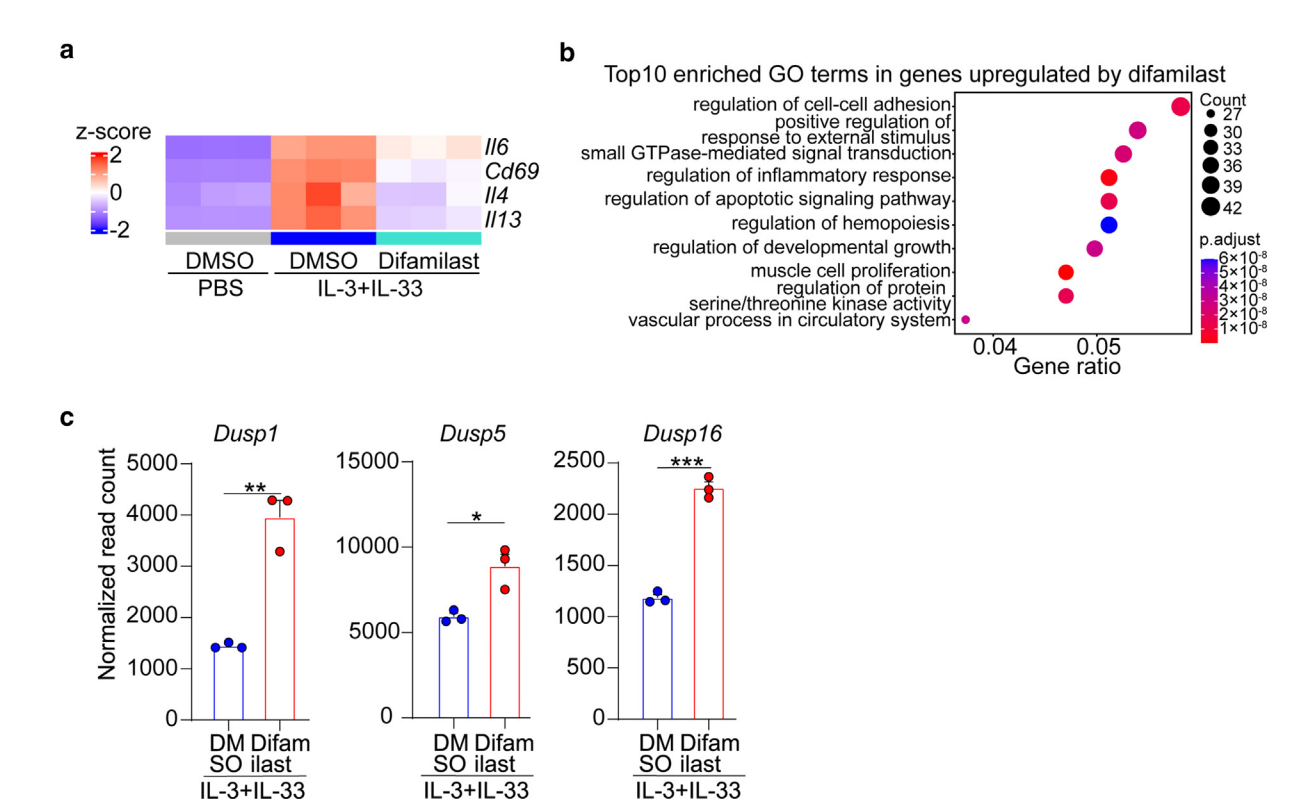
Supplementary Figure S3. Difamilast inhibits IL-4 production and degranulation of BMBAs stimulated in vitro with IgE/allergen. (a) BMBAs sensitized with TNP-IgE were stimulated by TNP-OVA or control OVA for 4 hours. The mRNA expression of indicated genes in stimulated BMBAs is shown. The value of mRNA expression in OVA-treated BMBAs was set as 1. (b) BMBAs sensitized with TNP-IgE were stimulated by TNP-OVA or control OVA for 6 hours in the presence of varying concentration of difamilast, GEBR-7b or vehicle DMSO. IL-4 concentration of BMBA supernatants is shown (mean ± SEM, n = 3). (c-d) BMBAs sensitized with TNP-IgE were stimulated by TNP-OVA or control OVA for 1 hour in the presence of difamilast (3 µM) or vehicle DMSO alone. In c, the surface expression of CD63 on BMBAs is shown in open histograms. Shaded histograms indicate control staining with isotype-matched antibodies. In d, the ratio of MFI, namely MFI of CD63 staining divided by MFI of control staining, is shown in each experimental group (mean  $\pm$  SEM, n = 3). Data shown in  $\mathbf{a}$ - $\mathbf{d}$  are representative of at least three independent experiments. \*P < .05, \*\*\*P < .001 measured by unpaired Student t test (for a), one-way ANOVA with Tukey multiple comparison test (for b) or two-way ANOVA with Tukey multiple comparison test (for d). MFI, mean fluorescence intensity; NS, not significant; OVA, ovalbumin; TNP-OVA, 2,4,6-trinitrophenol-conjugated ovalbumin.



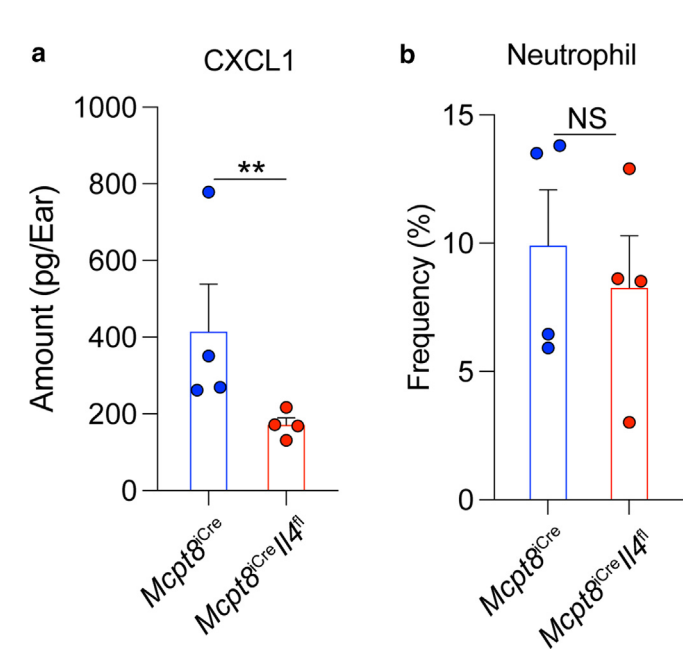
Supplementary Figure S4. Re-analysis of single-cell RNA-seq data of OX-induced AD-like skin lesion. Publicly available single cell RNA seq data (GEO accession number: GSE149121) were re-analyzed. (a) UMAP plot of the ethanol-treated and OX-treated skins are shown. Colors indicate different Seurat clusters. (b) Feature plots showing the expression of *II4* and *CxcI1* in the OX-treated skin are shown. *II4* was predominantly expressed in basophils (cluster 12), whereas *CxcI1* was predominantly expressed in fibroblasts (cluster 20 and 22). (c) Ligand-receptor interactome analysis was conducted on datasets of the OX-treated skins. Heatmap showing the relative importance of each cluster based on the computed network centrality measures of IL-4 signaling pathway. Interactome analysis inferred that the major sender of IL-4 signaling was basophils (cluster 12), whereas the major receiver was monocyte-macrophages (cluster 0), cDCs (cluster 11 and 13) and fibroblasts (cluster 20 and 22). DC, dendritic cell, DETC, dendritic epidermal T cell; ILC, innate lymphoid cell; OX, oxazolone; UMAP, Uniform Manifold Approximation and Projection.



Supplementary Figure S5. Difamilast treatment shows little or no effect on the surface expression of IL-3Ra, FceRla, and IL-33R as well as the cell viability. (a and b) BMBAs were treated with difamilast (3 µM) or vehicle DMSO for 6 hours and subjected to flow cytometric analysis. In a, CD200R3<sup>+</sup>CD49b<sup>+</sup> basophils among the c-Kit' population in the BMBAs were gated (left panels), and surface expression of IL-3Ra, FceRIa, and IL-33R (right panels) are shown in open histograms. Shaded histograms in the right panels indicate staining with isotype-matched control antibodies. In b, the ratio of MFI, namely MFI of CD63 staining divided by MFI of control staining, is shown in each experimental group (mean  $\pm$  SEM, n = 3). (c) BMBAs were stimulated for 6 hours by IL-3 + IL-33 or control PBS (left panel), and TNP-OVA or control OVA (right panel) in the presence of difamilast (3 µM) or vehicle DMSO. The frequency of Acridine orange<sup>+</sup> DAPI<sup>-</sup> live cells among total Acridine orange<sup>+</sup> cells is shown (mean  $\pm$  SEM, n = 3). Data shown in **a**–**c** are representative of at least three independent experiments. NS: not significant measured by unpaired Student t test (for b) or two-way ANOVA with Tukey multiple comparison test (for c). BMBA, bone marrow—derived basophil; NS, not significant; TNP-OVA, 2,4,6-trinitrophenol-conjugated ovalbumin; MFI, mean fluorescence intensity.



Supplementary Figure S6. Difamilast treatment upregulates the dual specificity phosphatases in IL-3 + IL-33-stimulated BMBAs. Bulk RNA-seq data in Figure 5a were analyzed. (a) A heatmap of indicated genes is shown. (b) The top 10 enriched GO terms in genes upregulated by difamiliast are plotted in order of gene ratio. The size of the dots indicates the number of genes associated with indicated GO terms while the color of the dots indicates the adjusted P-values (p. adjust) calculated by one-sided Fisher exact test with Benjamini-Hochberg correction. (c) Normalized counts of the indicated genes are shown (mean  $\pm$  SEM, n = 3 each). \*P < .05, \*\*P < .01, \*\*\*P < .001 measured by unpaired Student t test.



Supplementary Figure S7. Basophil-specific IL-4-deficiency reduces the amounts of CXCL1 in the OX-treated skin, but not the frequency of circulating neutrophils. (a) Mcpt8<sup>iCre</sup> Il4<sup>fl</sup> and control Mcpt8<sup>iCre</sup> mice were treated with OX as in Figure 1. The amounts of CXCL1 in tissue homogenates collected from OX-treated skin lesion on day 8 are shown (mean  $\pm$  SEM, n =4 mice each). (b) The frequency of neutrophils among CD45<sup>+</sup> cells in the peripheral blood of Mcpt8<sup>iCre</sup> II4<sup>fl</sup> and control Mcpt8<sup>iCre</sup> mice under homeostatic condition is shown (mean  $\pm$  SEM, n = 4 mice each). \*\*P < .01, NS: not significant measured by unpaired Student t test (for **a** and **b**). NS, not significant.